Experimental Evaluation and Upper-Bounds of Cross-Sensitivity in Stacked RFID Sensors

Francesca Maria Chiara Nanni, *IEEE Graduate Student Member*, Gaetano Marrocco, *IEEE Senior Member*

***Abstract*—The dense distribution of wireless sensors based on Ultra-High-Frequency (UHF) Radio-Frequency Identification (RFID) technology, in the food market or drug cold chains, raises issues regarding the effects of mutual electromagnetic coupling on sensing. In the case of stacked items, in fact, inter-antenna coupling can cause disturbance to sensor measurements, thus affecting the specificity and reliability of the collected data. This paper experimentally investigates the effects of coupling for some configurations of antenna size and alignments by exploiting capacitive sensing based on the emerging auto-tuning integrated circuit (IC) architectures. The results revealed that electromagnetic coupling typically induces cross-sensitivity and instability so that the variation of any sensor's output will also be indirectly captured by adjacent devices. However, this disturbing effect vanishes after a threshold decoupling distance of the order of 4 mm for a small-footprint loop (15mm×15mm), and 15 mm in the case of a card-like footprint (C-dipole, 54mm×16mm). Moreover, experiments revealed that the above distances can be halved by resorting to a 180° rotation of the adjacent items.**

***Index Terms*—Logistics, RFID, electromagnetic coupling, self-tuning technology, cross-sensitivity.**

I. Introduction

Besides inventory, item-level monitoring is becoming critical in the food and pharmaceutical industries, as it ensures safety, quality, and compliance with regulatory standards. In the food market, effective surveillance helps preventing contamination, spoilage, and spread of foodborne diseases [1], while allowing timely corrective actions, recalls, or withdrawals [2]. Similarly, in the pharmaceutical chain, proper values of environmental parameters such as temperature, humidity, and light exposure must be guaranteed to ensure the efficacy, safety, and integrity of medicinal products [3], [4], [5], [6].

The advent of the Internet of Things (IoT) is currently providing an opportunity to improve traditional drug distribution methods to ensure efficient item-level monitoring and prevent adverse events. In particular, Radio Frequency Identification (RFID) technology is an attractive option for next-generation industrial IoT settings due to low-power passive wireless communication with the additional benefits of low cost, disposability, real-time tracking, and overall improved customer service [7]. However, the cold chain and the storage of medicines will require managing a dense distribution of electronic labels [8], [9], such as stacks of drug packages or small bottles, but even at sub-package levels, when multiple blisters, phials, drug sachets [10] inside the same box must be individually labeled and monitored. The above dense arrangements force the proximity of the antennas and ICs, leading to coupling interactions, which are typical of multi-sensing systems. Mutual coupling potentially degrades communication performance [11], namely it is responsible for a reduction of the reading distance, but also of the signal-to-interference-plus-noise ratio (SNIR) [12], [13], which makes the communication less stable. Furthermore, if the label is provided with sensors, there is an additional risk of cross-talk [14], which can lead to inaccurate measurements and data misinterpretation.

The authors are with the Pervasive Electromagnetics Lab, University of Rome Tor Vergata, Via del Politecnico 1, Rome 00133, Italy (e-mail: francesca.nanni@alumni.uniroma2.eu, gaetano.marrocco@uniroma2.it)

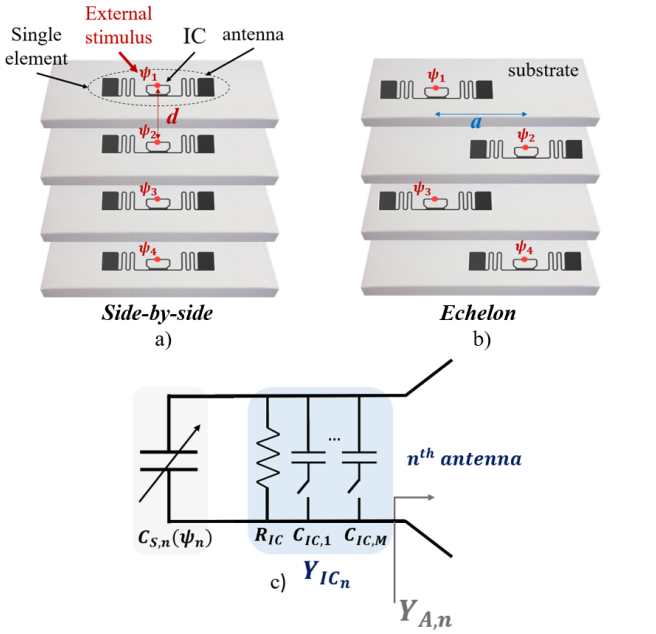

Fig. 1. Sketch of RFID sensors over stacks of items. Two alignment options are considered: a) *side-by-side* and b) *echelon arrangements*. c) Equivalent circuit of an RFID node comprising an external capacitive sensor $C_{S,n}$ and an auto-tuning IC.

The effects of mutual coupling among RFID antennas were theoretically investigated in [15], concerning the communication and the identification issues, and then experimentally verified in [16] by introducing the concept of RFID grid. The electromagnetic parameters of RFID antennas are strongly interconnected and deterministic tools were provided to estimate the communication performance. More recently, the statistical investigation in [17] confirmed the non-negligible impact of the coupling on the received power at the chip level.

RFID sensing introduces, moreover, additional degrees of complexity and is still an open research issue. In particular, this paper will focus on a family of RFID sensing architectures involving auto-tuning microchips, since the electromagnetic

coupling effect is more relevant, and this arrangement can hence be considered a worst-case scenario. A general theoretical electromagnetic model of auto-tuning RFID ICs was presented in [18] for a single-chip device and developed further in [19] for near-field reader-to-tag communication. This adaptive technology was also used for the wireless monitoring of AC currents [20], electrolytes [21], temperature [22], and finally exploited by the interface with external potentiometric sensors [23]. The coupling between two auto-tuning antennas was then theoretically and numerically described, for the first time, in [24] by means of a two-port network but without accounting for sensing issues. Finally, the authors recently presented some preliminary experiments with two small loops [25], which confirmed the presence of "cross-sensitivity". Now, by extending the results in [25], we will consider a new general stack of both small and large labels with different alignments, with the purpose of evaluating the effects of coupling on sensing (Fig. 1), and in particular the cross-sensitivity and the decoupling distance. An experimental campaign has been carried out by exploiting sensor antennas of different sizes and for different inter-antenna and alignment strategies with the purpose of quantifying the effects and, above all, identifying the upper bound performance and providing indications to select the best placement of antennas in stacking configurations.

The structure of this paper unfolds as follows: Section II formalizes the problem and expands the auto-tuning model to include coupled RFID antennas [15] and introduces the related performance metrics. Section III describes the planning of the experimental campaign and the considered test configurations, while Section IV introduces the measurement setup and the adopted materials. The achieved experimental results are analyzed in Section V, and finally, some countermeasures are derived to minimize the effects of coupling.

II. Statement of the problem

Without loss of generality, let us focus on a stack of equally spaced RFID antennas by a distance $d<<\lambda$.

This arrangement can be considered as a worst case for the coupling since sensing periodic scatterers may sustain Floquet modes [26] that amplify the inter-element interaction.

Each antenna should be equipped with an interdigitated capacitor (IDC) that acts as the capacitance $C_{S,n}$ sensor. Such an IDC can eventually be coated with some chemically interacting material (CIM), as in [27], to achieve specificity of sensing to particular local conditions. The parallel cascade of the antenna and the IDC is in turn connected to a radio-frequency IC transponder IC_n that is provided with auto-tuning capability, as better described later on.

Let $\mathbf{\Psi} = \{\psi_1, ..., \psi_N\}$ be a set of local external stimuli, such as humidity, temperature, pH, ammonia, amines or other volatile compounds, each of them interacting with the proper sensing IDC$_n$. The IDC of the antennas could be all different, namely IDC$_n$ will sense just ψ_n, or instead they will all sense the same stimuli, for instance, the microclimate (temperature and humidity) inside the same package. However, the sensors are such that the presence/variation of ψ_n will produce a change in the $C_{S,n}(\psi_n)$ capacitance. By assuming that the cascade of the antenna plus the IDC is initially matched to the RF admittance, $Y_{IC,n}$, of its microchip, the variation of the sensor capacitance will produce an admittance mismatch that the IC auto-tuning circuit will partially compensate according to the following procedure. The IC is provided with a voltage-controlled capacitor that can span between a discrete set of values as follows:

$$C_{IC}(s_n) = C_{IC,0} + s_n C_{IC,step} \tag{1}$$

where the offset $C_{IC,0}$ and the step $C_{IC,step}$ are manufacturer-specific. The integer number "s_n", hereafter referred as *sensor code,* indicates the re-tuning effort and is returned by the IC following a standard RFID query. The term s_n is hence indirectly related to external stimuli, since the internal capacitance of the IC is automatically adjusted to cancel the instantaneous variation of the total susceptance of the device, namely the parallel connection of the sensing capacitor and the input susceptance B_A of the antenna (assumed to be insensitive to the external environment), so that the following metrics is minimized:

$$|C_{IC}(s_n) + B_{A,n}/\omega + C_{S,n}(\psi_n)| \to 0 \tag{2}$$

where $\{B_{A,n}\}$ are the input susceptances of the antennas.

By inverting (2), the re-tuning indicator s_n is found to be directly proportional to $C_{S,n}(\psi_n)$ and hence related to the physical parameter ψ_n:

$$s_n(\psi_n) = S_{min} + nint\left(-\frac{(C_{IC}(S_{min}) + B_{A,n}/\omega + C_{S,n}(\psi_n))}{C_{IC,step}}\right). \tag{3}$$

The allowed auto-tuning effort is generally limited so that the sensor code will vary within the range $S_{min} < s_n < S_{max}$, S_{min} and S_{max} being dependent on the implementation of the IC. In case of a more severe mismatch, the sensor code saturates to the nearest boundary value.

Due to the proximity among antennas, they will be subjected to electromagnetic mutual coupling so that their input susceptances $\{B_{A,n}\}$ will be overall inter-dependent and the stack can be considered as a multi-port network, or an RFID grid [15], [16]. Accordingly, the output set $\{s_n\}$ of the sensing procedure is expected, from (3), to experience some effects of the coupling, namely *i*) instability in the auto-tuning, and *ii*) cross-sensitivity. Cross-sensitivity means that the output of the *n*-th device is related to those of the others, thus reducing the specificity of each sensor, the resolution, and the overall robustness of the sensing system.

The goal of the following experiments is to quantify the effect of cross-coupling and identify the mutual distance threshold after that the instabilities and the cross-sensitivity become negligible. For this purpose, we introduce the following metrics that are computed starting from the output sensor code of the stack of sensors:

1) *Averaged sensor codes* ($\overline{s}_n$) over a 50-samples moving window. The number of samples is chosen to ensure the extinction of transient phenomena in the auto-tuning response due to abrupt changes in boundary conditions nearby the antenna [28];

2) *Baseline (β_n):* the mean value of the sensor code for 50 samples under a reference boundary condition $\{\psi_n = \psi_{n,0}\}$. As each IC will have to dynamically auto-tune during a transient when all the coupled ICs are doing the same, the system is not stable and this baseline is expected to be noisy;
3) *Swing (χ):* the standard deviation of the output signal over 50 time samples. An increase of χ will induce a degradation of the resolution of the sensors, thus reducing the levels they will be able to recognize;
4) *Differential sensor code* ($\triangle s_n = \overline{s}_n - \beta_n$): the averaged output value of the sensor with respect to the baseline. This parameter will provide a measure of to what extent the proximity among antennas will affect the dynamic response to a variable external stimulus;
5) *Cross-sensitivity (σ_{ij}):* the dependence of each sensor on the local change in boundary conditions that, in turn, affects the other devices. It corresponds to the off-diagonal terms of the sensitivity matrix $\boldsymbol{\sigma}$ defined in (4). Instead, the main diagonal terms are referred to as *self-sensitivities*.

$$\boldsymbol{\sigma} = \begin{bmatrix} \sigma_{11} & \cdots & \sigma_{1N} \\ \vdots & \ddots & \vdots \\ \sigma_{N1} & \cdots & \sigma_{NN} \end{bmatrix} = \begin{bmatrix} \frac{ds_1}{d\psi_1} & \cdots & \frac{ds_1}{d\psi_N} \\ \vdots & \ddots & \vdots \\ \frac{ds_N}{d\psi_1} & \cdots & \frac{ds_N}{d\psi_N} \end{bmatrix}. \tag{4}$$

The elements of the matrix are evaluated by assuming a linear model, as proven acceptable in [23] for small voltage variations, $\psi_m \leftrightarrow s_n$ such that $\sigma_{nm} \approx (\Delta s_n(\psi_{m,max}) - \Delta s_n(\psi_{m,min}))/(\psi_{m,max} - \psi_{n,min})$;
6) *Decoupling distance:* the inter-element threshold distance

$$d = d_{th} \tag{5}$$

above that the cross-sensitivity and the swings are less than 50% of the corresponding unperturbed values.

III. Test Stacks

We focus the experimental investigation on some combinations of a number of devices in the stack, the size (footprint) of antennas, their mutual distance, and alignment. In all cases, for simplicity and reproducibility of implementation, the variation of the IDC is emulated by resorting to a varactor diode, whose equivalent sensing capacitance can be externally controlled by a polarization voltage $V_{P,n}$. Accordingly, the $\{\psi_n\}$ stimuli will here correspond to the polarization voltages. The details of devices and instrumentation are given in Section IV.

We consider the following options:

i) two footprints for the sensor antenna: small (S: 14.4×15.1 mm^2) and large (L: 100×504 mm^2);

ii) two alignments of devices in the stack: *side-by-side* like, namely, contiguous stacked elements are fully coaxial, and *echelon*, where contiguous stacked elements are alternatively offset transversely. The latter corresponds, for instance, to packages that are mutually rotated by 180°.

The three considered tests are described next. In all cases, experiments were carried out when only the bottom device was polarized ($V_{P,1} \neq 0$, $V_{P,m} = 0$, $m = 2, .., N$). The baseline (corresponding to $V_{P,m} = 0$ for all m) was also evaluated as a reference. Measurements were repeated three times for each configuration to ensure the reproducibility of the results under specific setup conditions, to which sensor code is particularly sensitive.

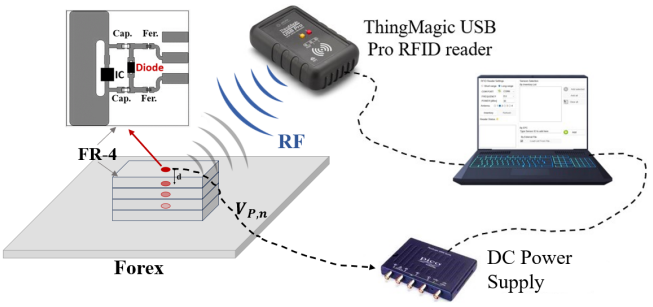

Fig. 2. Experimental setup for the interrogation of the stack of sensors also including the voltage supply for polarizing the varactor diode over any RFID node.

A. Test 1: impact of the number of devices

A stack of up to four coaxial devices in a case of very close spacing, d = 2 mm (Fig. 1 a) and b)). The antenna size is the smaller one. This arrangement is very extreme and could emulate the case of tagged medicine sachets in a package. The goal is to analyze the impact of the length of the stack on the baseline, swing, and cross-sensitivity.

B. Test 2: impact of device footprint

A stack of four coaxial devices with increasing mutual distance when just one device is dynamically polarized, while the remaining are unpolarized. Both small- and large-size antennas are considered. The goal is to evaluate: *i)* the decoupling threshold distance (d_{th}) after that the above metric becomes stable, and *ii)* its relationship with the antenna footprint.

C. Test 3: impact of stack alignment

The four-element stacks as in the previous test in the case of alternate alignment with vertical and horizontal inter-element distances equal to $d = a = d_{th}/2$. Both small and large antennas are considered. The goal is to verify the effectiveness of the alternate alignment to mitigate the coupling effect even for very small inter-element separation.

IV. Experimental set-up

The experimental setup is described in Fig.2 and comprises a DC power supply, which acts as a voltage source to polarize the varactor, and an RFID reader that interrogates the prototypes under test.

A. Sensor Antennas

The small and large antennas are derived from [23] (Fig. 3). Both include a copper loop on an FR-4 substrate and additional traces to allocate the microchip, varactor, decoupling capacitors, and ferrite beads.

TABLE I
SIZES OF THE CONSIDERED LOOP ANTENNAS.

$loop$	$l[mm]$	$q[mm]$
1	6.5	2.1
2	8.5	1.1
3	10.2	2.1
4	6.5	1.1

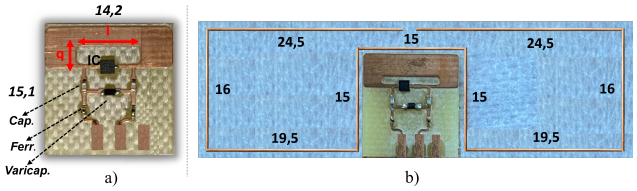

a) b)

Fig. 3. a) Layout detail of the two kinds of considered antennas hosting the sensing capacitor. a) Small Antenna: a square loop on FR-4 substrate (ε_r= *4.3, tanδ = 0.025,* size: *14.2×15.1 mm*^{2}, thickness *1.6 mm).* b) Large antenna including a boosting copper wire dipole on a closed-cell PVC foam board, (ε_r *= 1.55,* σ*= 0.0006 S/m,* size *100×504 mm*^{2}, thickness *5 mm*) not visible in the sketch.

For the sake of generality, the aspect ratios of the four loop antennas are a little different and are reported in Tab.I.

The larger antenna also includes a copper wire booster (radius 0.8 mm), housed on a polymeric substrate (closed-cell PVC foam board), which is inductively coupled to the loop to increase the radiation gain. The overall size are 15×15 mm^2 (small antenna) and 54×16 mm^2 (large antenna), respectively.

Stacks are emulated by polystyrene spacers of increasing thickness.

B. Microchip

Currently, to the best knowledge of the authors, the only IC available on the market provided with auto-tuning capability with a large enough dynamics to enable sensing is the Axzon Magnus-S3 [29]. The related parameters are $C_{IC,0} = 1.9\ pF$, $C_{IC,step} = 3.1\,fF$, conductivity $G_{IC} = 0.482\,mS$, $S_{min} = 80$, $S_{max} = 400$, and nominal power sensitivity $p_{IC} = -16.6\,dBm$.

C. Varactor Diode

The varactor diode to emulate the variations of the sensing capacitance $C_{S,n}$ is the SMV1405 (vendor [30], [31]) having a $V_P - C_S$ curve:

$$C_S(V_P) = \frac{C_{J0}}{(1 + \frac{V_P}{V_J})^M} \tag{6}$$

where $\{C_{j0}, M, V_J\}$ are the capacitance of the diode when it is not polarized, a constant dependent on the material, and the barrier potential, respectively.

The polarization device is a DC voltage source, namely the PicoScope 2000 [32].

D. Interrogating Reader

The interrogation device to collect the sensor codes is the ThingMagic USB-Pro equipped with an internal linearly polarized patch antenna (Fig. 2). The reader is controlled by a custom software which also returns the sensor-code.

TABLE II
A) MEAN VALUE AND STANDARD DEVIATION OF EACH DEVICE WHEN UNLOADED AND ISOLATED FROM THE OTHERS VERSUS B) THE SAME VALUES WHEN ALL THE FOUR DEVICES ARE STACKED AT A DISTANCE OF *d=2 mm* AND UNLOADED.

IC	β	χ
1	75	4.9
2	55	14.3
3	179	7.8
4	249	13.5

a)

IC	β	χ
1	166	94
2	127	69
3	444	24
4	295	46

b)

V. RESULTS

A. Test 1: impact of the number of devices

Tab.II shows the sensor codes of the four antennas in standalone and stacked configurations, but without voltage polarization of the varactors. Due to the different sizes of the loop antennas, the measured baselines are specific to each antenna, even in isolated configurations. The proximity of the antenna strongly impacts the sensor code baselines that become roughly doubled with respect to standalone configurations (Tab.II). An even more relevant effect is visible on the swing, which, in some cases, rises by an order of magnitude, thus producing uncertainty in the measurements.

When one of the small antennas is polarized according to a staircase profile (Fig. 4.a) with steps $V_P = \{1V, 2V, 3V\}$, the response of that antenna follows the stimuli with a swing that increases along with the number of elements in the stacks, thus making the identification of the levels more and more challenging (Tab.III). For example, moving from a single antenna to four stacked antennas, χ_1 rises from 3 to 67. The self-sensitivity σ_{11} is slightly degraded (from 100 units/volt to 96 units/volt). The trend is not monotonic with the number of elements. The cross-sensitivity is moderate in the case of just two closely spaced devices (7 units/Volt), but other values are comparable to the self-sensitivity in the case of three and four antennas. However, the effect mainly disturbs antennas that are close to the polarized ones.

The case of large antennas (Fig. 4.b) also shows that as the number of elements increases, the swing increases by about 20 units, although in general, it turns out to be more modest with respect to smaller antennas (details resumed in Tab.IV). Self-sensitivity, on the other hand, appears to decrease as the number of antennas increases, going from a value of 85 to 45.

B. Test 2: impact of device footprint

For small antennas (Fig.5.a)), the cross-sensitivity practically cancels and the swing stabilizes (except for the *n* = 3 antenna) just after the distance $d = d_{th,S} = 4mm$. For the larger antenna, the decoupling distance is instead roughly $d_{th,L} = 15mm$. The swing of the polarized one, however, is less impactful than that in the case of small antennas. The longer decoupling distance with respect to the smaller footprint antenna is probably due to the more extended near-field regime of the large antenna, which is related to the antenna size, so that the disturbing effect is more persistent, even at larger inter-antenna distances.

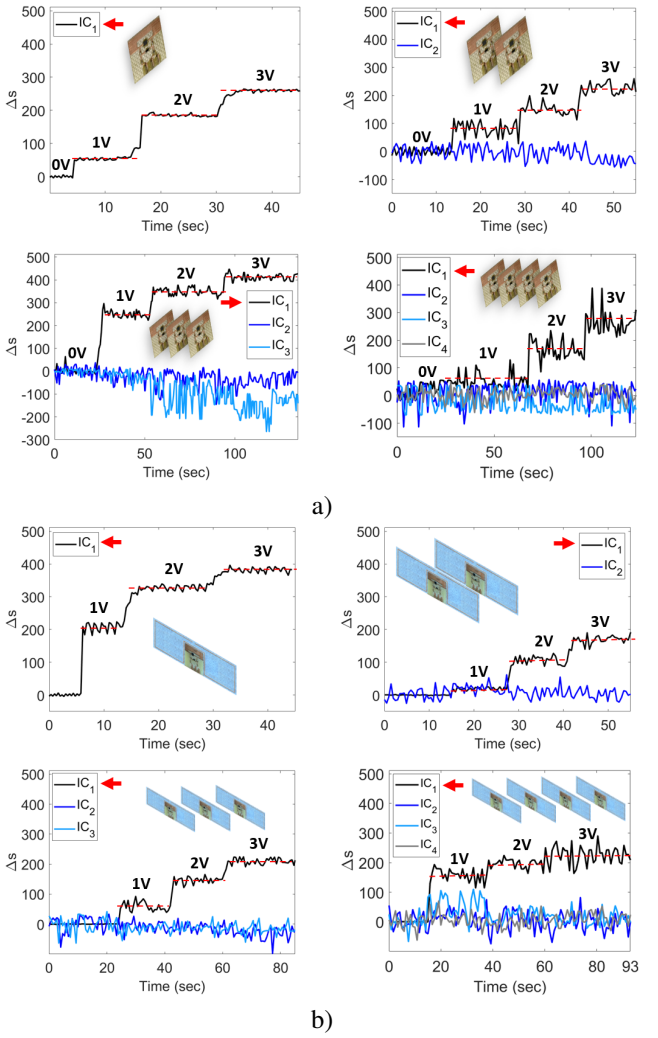

Fig. 4. Test 1 - Measured differential sensor codes for a stack of *a)* small antennas, and *b)* large antennas, mutually spaced d=2mm, when just the bottom antenna (n=1) is polarized by a staircase voltage profile $V_P = \{1V, 2V, 3V\}$. The dashed lines are for the average values, while the arrows in the legends indicate the polarized device.

Fig. 6 and Fig. 7 finally show some examples of the four-element stacks of the larger antennas with inter-element threshold distance $d_{th,L} = 15$ mm in the case of: *i)* a single device is sequentially polarized (Fig. 6) and *ii)* two devices (#1 and #3) are simultaneously and independently polarized. In both configurations, the response is rather stable, and all the other unpolarized devices are insensitive to changes in the polarized ones.

C. Test 3: impact of stack alignment

From the profiles in Fig.8, the performance metrics are extracted and compared with the corresponding value of coaxial configurations involving larger inter-element spacing d_{th} (Fig. 9). When the alternate alignment of the stack of devices is exploited, the level of cross-sensitivity and swing are comparable to the values obtained in a coaxial decoupled configuration and kept low even for half of the decoupling inter-element distance. This suggests that the decoupling distance constraint

TABLE III
MEASURED BASELINES AND CROSS-SENSITIVITIES OF STACKED OF A) ONE, B) TWO, C) THREE, AND D) FOUR SMALL DEVICES WITH AN INTER-ELEMENT DISTANCE OF D = 2 MM.

IC	χ	σ_{n1}
1(*polarized*)	3.5	101

a)

IC	χ	σ_{n1}
1(*polarized*)	20.1	70
2	25,4	-7

b)

IC	χ	σ_{n1}
1(*polarized*)	16.4	84
2	34.7	-65
3	45.8	-8

c)

IC	χ	σ_{n1}
1(*polarized*)	67	96
2	36	-19
3	30	6
4	32.4	8

d)

TABLE IV
MEASURED BASELINES AND CROSS-SENSITIVITIES OF STACKED CONFIGURATION OF A) ONE, B) TWO, C) THREE, AND D) FOUR LARGE DEVICES WITH AN INTER-ELEMENT DISTANCE OF D = 2 MM.

IC	χ	σ_{n1}
1(*polarized*)	7.3	85

a)

IC	χ	σ_{n1}
1(*polarized*)	14.9	77
2	15.9	-11

b)

IC	χ	σ_{n1}
1(*polarized*)	13.2	76
2	18.4	-12
3	17.4	1

c)

IC	χ	σ_{n1}
1(*polarized*)	23.5	45
2	30	-8
3	28.2	-23
4	23.2	2

d)

for both footprints can be effectively addressed by arranging the devices alternately, even at shorter spacings.

VI. CONCLUSIONS

By the help of an experimental campaign, this paper has analyzed the effects of coupling between sensors equipped with auto-tuning technology. Experiments have shown striking differences in the case of antennas with large and small footprints, such as:

1) the threshold decoupling distance is smaller in the case of smaller-size antennas ($d_{th,S} = 4$mm $< d_{th,L} =$ 15mm). This suggests the use of smaller footprint-devices whenever possible;
2) in the case of large antennas very close to each other, the achievable sensing resolution is worse with respect to smaller antennas. As a result, discriminating fine

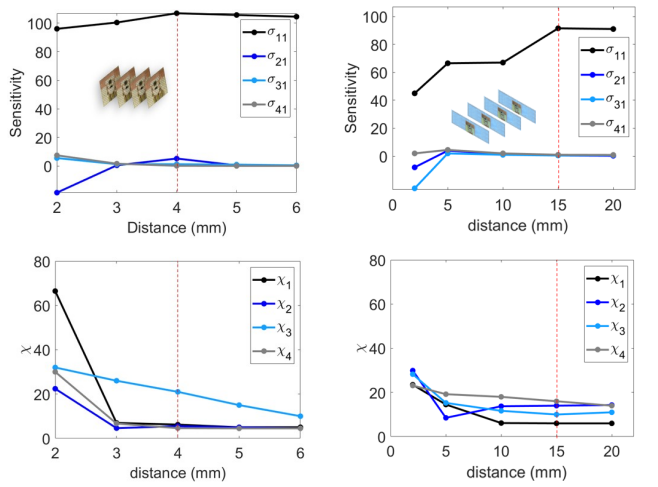

Fig. 5. Test 2 - Measured self- and cross-sensitivities $\sigma_{1n}(d)$ and swings $\chi_{1n}(d)$ n=1,..,4 for stack of coaxial *a)* small antennas, and *b)* large antennas, versus increasing spacing. The bottom antenna (n=1) is the polarized one.

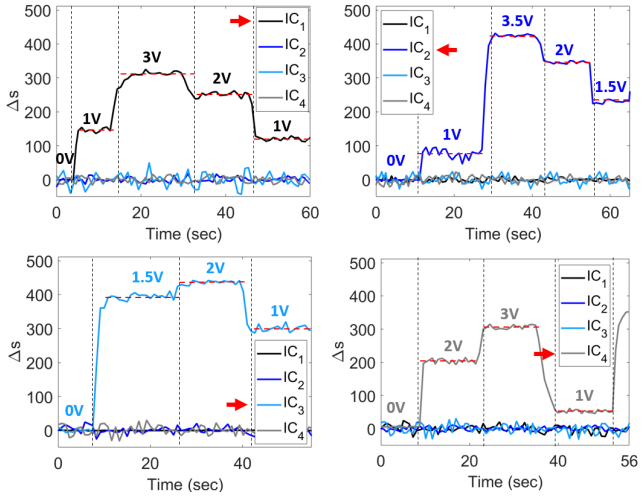

Fig. 6. Test 2 - Example of differential sensor codes for a stack of four large devices that are mutually spaced by the decoupling distance $d_{th,L} = 15mm$. Just a sensor at a time is polarized (tagged with an arrow in the legends) with a non-monotonic sequence of voltages V_P. The dashed lines are for the average values, while the arrows in the legends indicate the polarized device.

variation of several environmental parameters becomes more challenging with respect to smaller devices;

The effects of coupling can be greatly mitigated by alternating the consecutive labels even for very short item-to-item distances. This could be practically achieved by an 180° rotation of adjacent items, without changing the position of the onboard labels. In case of coarser alignments of the antennas on the items, we can expect that the disturbing effect will be localized around consecutive sensors, especially if the illumination footprint of the reader will activate only a subset of the grid at a time, and if the content of the items has losses that prevent system resonances and induces a natural decoupling.

The study focuses on loops due to their common adoption as RFID antennas, either as a standalone radiating elements or as

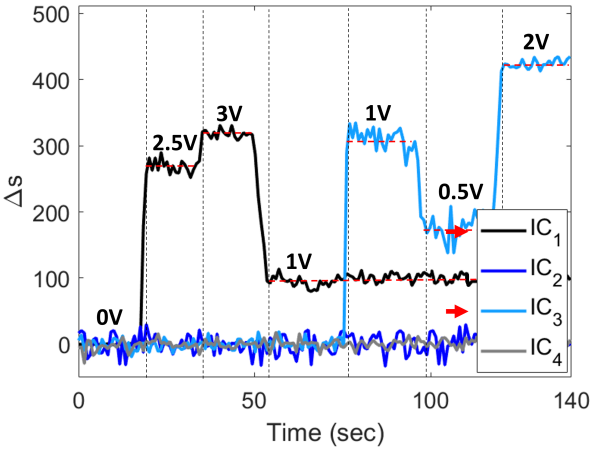

Fig. 7. Test 2 - Example of differential sensor codes for a stack of four large devices that are mutually spaced by $d_{th,L} = 15mm$, when two sensors are simultaneously excited by two independent voltage sources. The dashed lines are for the average values, while the arrows in the legends indicate the polarized devices.

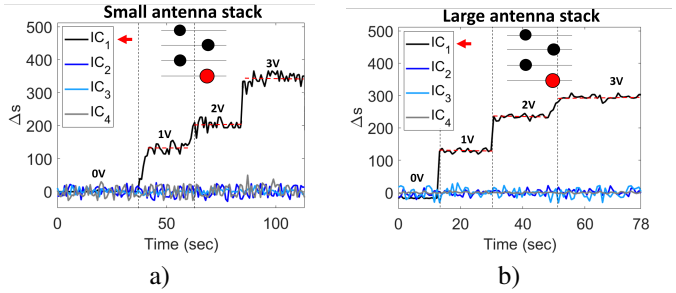

Fig. 8. Test 3 - Differential sensor codes for four a) small and b) large devices in *echelon* configuration so that the vertical and horizontal inter-antenna distance is $d = a = d_{th}/2$=7.5 mm. Only the bottom antenna is polarized.

part of impedance adapters (T-match, gamma-match, and loop-match) in RFID applications. Furthermore, the loop, which hosts intense currents, significantly influences the antenna behaviors, as the correlated results between small loops and larger loop-matched dipoles confirm. The findings may extend to dipole-like antennas with loop-based adapters. Considerations on other radiators, like patches or slots, would deserve dedicated experimentations.

ACKNOWLEDGMENT

Work partly funded by European Union - NextGenerationEU, ECS 0000024 Rome Technopole, CUP B83C22002820006, PNRR Mission 4, Component 2, Investment 1.5.

REFERENCES

[1] H. Yousefi, H.-M. Su, S. M. Imani, K. Alkhaldi, C. D. M. Filipe, and T. F. Didar, "Intelligent food packaging: A review of smart sensing technologies for monitoring food quality," *ACS sensors*, vol. 4, no. 4, pp. 808–821, 2019.

[2] B. Bhavadharini, M. Kavimughil, B. Malini, A. Vallath, H. K. Prajapati, and C. Sunil, "Recent advances in biosensors for detection of chemical contaminants in food, a review," *Food Analytical Methods*, vol. 15, no. 6, pp. 1545–1564, 2022.

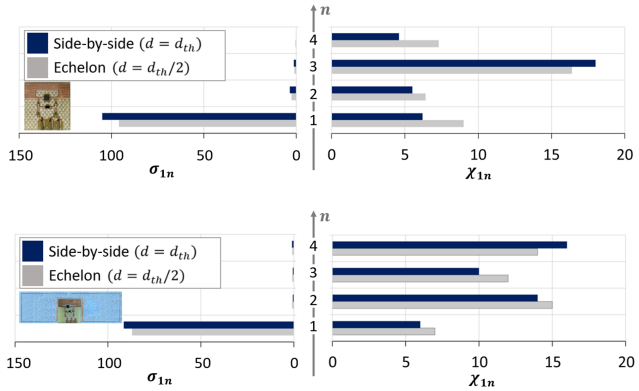

Fig. 9. Test 3 - Resuming bars for stacks of four small and large antennas with two different inter-element distances, $d = d_{th}$ for the *side-by-side* and $d = d_{th}/2$ for the *echelon* alignment.

[3] N. Kumar and A. Jha, "Temperature excursion management: A novel approach of quality system in pharmaceutical industry," *Saudi Pharmaceutical Journal*, vol. 25, no. 2, pp. 176–183, 2017. [Online]. Available: https://www.sciencedirect.com/science/article/pii/S131901641630069X

[4] D. Masi, S. Amendola, N. D'Uva, C. Miozzi, G. Bianco, C. Occhiuzzi, and G. Marrocco, "Radio-pill: Rfid miniaturized and battery-free humidity probe for pharmaceutical moisture analysis," in *2022 IEEE 12th International Conference on RFID Technology and Applications (RFID-TA)*, 2022, pp. 153–156.

[5] M. Safkhani, S. Rostampour, Y. Bendavid, and N. Bagheri, "Iot in medical & pharmaceutical: Designing lightweight rfid security protocols for ensuring supply chain integrity," *Computer Networks*, vol. 181, p. 107558, 2020.

[6] N. D'Uva, F. Camera, S. Amendola, S. Nappi, C. Miozzi, C. Occhiuzzi, and G. Marrocco, "Batteryless wireless temperature/humidity sensor for item-level smart pharma packaging," in *2021 IEEE International Workshop on Metrology for Industry 4.0 and IoT (MetroInd4.0 and IoT)*, 2021, pp. 145–149.

[7] G. Casella, B. Bigliardi, and E. Bottani, "The evolution of rfid technology in the logistics field: a review," *Procedia Computer Science*, vol. 200, pp. 1582–1592, 2022.

[8] Y.-Y. Chen, Y.-J. Wang, and J.-K. Jan, "A novel deployment of smart cold chain system using 2g-rfid-sys," *Journal of Food Engineering*, vol. 141, pp. 113–121, 2014.

[9] F. Li and Z. Chen, "Brief analysis of application of rfid in pharmaceutical cold-chain temperature monitoring system," in *Proceedings 2011 International Conference on transportation, mechanical, and electrical engineering (TMEE)*. IEEE, 2011, pp. 2418–2420.

[10] S. Ting, S. K. Kwok, A. H. Tsang, and W. B. Lee, "Critical elements and lessons learnt from the implementation of an rfid-enabled healthcare management system in a medical organization," *Journal of medical systems*, vol. 35, pp. 657–669, 2011.

[11] H. Yojima, Y. Tanaka, Y. Umeda, O. Takyu, M. Nakayama, and K. Kodama, "Analysis of read range for uhf passive rfid tags in close proximity with dynamic impedance measurement of tag ics," in *2011 IEEE Radio and Wireless Symposium*. IEEE, 2011, pp. 110–113.

[12] M. A. Jensen and J. W. Wallace, "A review of antennas and propagation for mimo wireless communications," *IEEE Transactions on Antennas and propagation*, vol. 52, no. 11, pp. 2810–2824, 2004.

[13] H. Luan, C. Chen, W. Chen, L. Zhou, H. Zhang, and Z. Zhang, "Mutual coupling reduction of closely e/h-plane coupled antennas through metasurfaces," *IEEE Antennas and Wireless Propagation Letters*, vol. 18, no. 10, pp. 1996–2000, 2019.

[14] P. Yang, J. Wang, H. Chen, Y. Li, W. Jiang, Y. Jing, R. Luo, and S. Qu, "Reducing cross-talk between two patch antennas using integrated electric metamaterials," in *2019 IEEE 2nd International Conference on Electronic Information and Communication Technology (ICEICT)*. IEEE, 2019, pp. 682–685.

[15] G. Marrocco, "Rfid grids: Part i-electromagnetic theory," *IEEE Transactions on Antennas and Propagation*, vol. 59, no. 3, pp. 1019–1026, 2011.

[16] S. Caizzone and G. Marrocco, "Rfid grids: Part ii, experimentations," *IEEE Transactions on Antennas and Propagation*, vol. 59, no. 8, pp. 2896–2904, 2011.

[17] A. Mughal, J. M. Sudersanan, S. Mostarshedi, B. Poussot, and J.-M. Laheurte, "Statistical evaluation of the coupling effects between tags in a uhf rfid forward link," *IEEE Journal of Radio Frequency Identification*, 2023.

[18] M. C. Caccami and G. Marrocco, "Electromagnetic modeling of self-tuning rfid sensor antennas in linear and nonlinear regimes," *IEEE Transactions on Antennas and Propagation*, vol. 66, no. 6, pp. 2779–2787, 2018.

[19] G. M. Bianco, S. Amendola, and G. Marrocco, "Near-field constrained design for self-tuning uhf-rfid antennas," *IEEE Transactions on Antennas and Propagation*, vol. 68, no. 10, pp. 6906–6911, 2020.

[20] I. Ullah, R. Horne, B. Sanz-Izquierdo, and J. C. Batchelor, "Rfid ac current sensing technique," *IEEE Sensors Journal*, vol. 20, no. 4, pp. 2197–2204, 2020.

[21] A. J. R. Hillier, V. Makarovaite, C. W. Gourlay, S. J. Holder, and J. C. Batchelor, "A passive uhf rfid dielectric sensor for aqueous electrolytes," *IEEE Sensors Journal*, vol. 19, no. 14, pp. 5389–5395, 2019.

[22] K. Zannas, H. El Matbouly, Y. Duroc, and S. Tedjini, "Self-tuning rfid tag: A new approach for temperature sensing," *IEEE Transactions on Microwave Theory and Techniques*, vol. 66, no. 12, pp. 5885–5893, 2018.

[23] F. Nanni and G. Marrocco, "Constrained design of potentiometric rfid sensors based on auto-tuning ics," *IEEE Sensors Journal*, vol. 23, no. 3, pp. 3050–3058, 2022.

[24] N. Panunzio and G. Marrocco, "A multi-port formulation for electromagnetic coupled auto-tuning rfid antennas," in *2021 XXXIVth General Assembly and Scientific Symposium of the International Union of Radio Science (URSI GASS)*. IEEE, 2021, pp. 1–4.

[25] F. Nanni, N. Panunzio, and G. Marrocco, "Cross-sensitivity of a dual-port potentiometric sensor based on auto-tuning rfid ics," in *2023 IEEE 13th International Conference on RFID Technology and Applications (RFID-TA)*, 2023.

[26] F. Lestini, N. Panunzio, G. Marrocco, and C. Occhiuzzi, "Epidermal rfid-based thermal monitoring sheet (r-tms) for microwave hyperthermia," *IEEE Journal of Electromagnetics, RF and Microwaves in Medicine and Biology*, pp. 1–10, 2023.

[27] S. Manzari, S. Pettinari, and G. Marrocco, "Miniaturised wearable uhf-rfid tag with tuning capability," *Electronics letters*, vol. 48, no. 21, pp. 1325–1326, 2012.

[28] F. Camera and G. Marrocco, "Electromagnetic-based correction of bio-integrated rfid sensors for reliable skin temperature monitoring," *IEEE Sensors Journal*, vol. 21, no. 1, pp. 421–429, 2020.

[29] Axzon, "RRFM3300-E Magnus-S3 M3E passive sensor IC," https://axzon.com/rfm3300-e-magnus-s3-m3e-passive-sensor-ic/, September 2021.

[30] Skyworks, "SMV1405 to SMV1430 Series - Plastic Packaged Abrupt Junction Tuning Varactors Datasheet," www.skyworksinc.com.

[31] Skyworks - Application Note, "Varactor SPICE Models for RF VCO Applications," www.skyworksinc.com.

[32] PicoScope, "Picoscope 2000 series datasheet," https://www.picotech.com/oscilloscope/2000/picoscope-2000-manuals.

Francesca Nanni received the B.S. and M.S. degree in Medical Engineering (Hons.) from the University of Rome Tor Vergata, Rome, Italy in 2019 and 2022, respectively. She is currently pursuing a Ph.D. degree in Computer Science, Control and Geoinformation within the Pervasive Electromagnetics Lab at the University of Rome Tor Vergata, and since July 2023 she is a part-time R&D Medical Engineer at RADIO6ENSE Srl. She is also part of the Cyber4Health project, which raises international awareness about the need to apply Cyber and Physical security by design in medical devices. She won the Best Student Paper Award at the 2022 IEEE International Conference on RFID Technology and Applications (RFID-TA 2022) and at the 2023 International Conference on RFID Technology and Applications (RFID-TA 2023).

Gaetano Marrocco (Senior Member, IEEE) is Full Professor of Electromagnetics Engineering at the University of Roma Tor Vergata, where he currently leads the Medical Engineering School. Since 2002, he has been a pioneer in Radiofrequency Identification and Sensing. His current research focuses on wireless-activated sensors, Wearable and Epidermal Electronics, and structural antennas for sensorized skins, smart prostheses, and finger augmentation devices for Tactile Internet. He serves as an Associate Editor of the IEEE Journal of Radiofrequency Identification and track Editor of the IEEE Journal of Flexible Electronics. Additionally, he chairs the Italian Section of URSI Commission D Electronics and Photonics and is a co-founder and president of the University spin-off RADIO6ENSE. RADIO6ENSE is actively involved in short-range electromagnetic sensing for Industrial Internet of Things, Smart Manufacturing, Automotive, and Digital Health. He is also listed in the PLOS 2022 ranking of the Top 2% Scientists Worldwide.